

Optical Engineering

OpticalEngineering.SPIEDigitalLibrary.org

Line scanning time-of-flight laser sensor for intelligent transport systems, combining wide field-of-view optics of 30 deg, high scanning speed of 0.9 ms/line, and simple sensor configuration

Masaharu Imaki
Shumpei Kameyama
Eitaro Ishimura
Masaharu Nakaji
Hideo Yoshinaga
Yoshihito Hirano

SPIE.

Masaharu Imaki, Shumpei Kameyama, Eitaro Ishimura, Masaharu Nakaji, Hideo Yoshinaga, Yoshihito Hirano, "Line scanning time-of-flight laser sensor for intelligent transport systems, combining wide field-of-view optics of 30 deg, high scanning speed of 0.9 ms/line, and simple sensor configuration," *Opt. Eng.* **56**(3), 031205 (2016), doi: 10.1117/1.OE.56.3.031205.

Line scanning time-of-flight laser sensor for intelligent transport systems, combining wide field-of-view optics of 30 deg, high scanning speed of 0.9 ms/line, and simple sensor configuration

Masaharu Imaki,^{a,*} Shumpei Kameyama,^a Eitaro Ishimura,^b Masaharu Nakaji,^b Hideo Yoshinaga,^c and Yoshihito Hirano^b

^aMitsubishi Electric Corporation, Information Technology R&D Center, 5-1-1 Ofuna, Kamakura, Kanagawa 247-8501, Japan

^bMitsubishi Electric Corporation, High Frequency and Optical Device Works, 4-1 Mizuhara, Itami, Hyogo 664-8641, Japan

^cMitsubishi Electric Corporation, Kamakura Works, 325 Kamimachiya, Kamakura, Kanagawa 247-8520, Japan

Abstract. We developed a line scanning time-of-flight (TOF) laser sensor for an intelligent transport system (ITS), which combines wide field-of-view (FOV) receiving optics of 30 deg and a high-speed microelectromechanical system scanner of 0.9 ms/line with a simple sensor configuration. The newly developed high-aspect ratio photodiode realizes the scanless and wide FOV receiver. The sinusoidal wave intensity modulation method is used for the TOF measurement. This enables the noise reduction of the trans-impedance amplifier by applying the LC-resonant method. The vehicle detection and axle counting, which are the important functions in ITS, are also demonstrated. © The Authors. Published by SPIE under a Creative Commons Attribution 3.0 Unported License. Distribution or reproduction of this work in whole or in part requires full attribution of the original publication, including its DOI. [DOI: [10.1117/1.OE.56.3.031205](https://doi.org/10.1117/1.OE.56.3.031205)]

Keywords: time-of-flight; phase detection; distance; range; LC tuning; microelectromechanical system; vehicle; axle.

Paper 161040SS received Jun. 30, 2016; accepted for publication Oct. 6, 2016; published online Oct. 20, 2016.

1 Introduction

Growing traffic congestion has made intelligent transport systems (ITS) vital for a safer and more efficient automobile society. In this system, the classification of the moving vehicle on the road is the key function, and vehicle detection and axle counting are especially important for the enhancement of this classification.^{1–5} The line scanning time-of-flight (TOF) laser sensor is an attractive tool for this detection and counting. This sensor can capture the cross section of a vehicle by laser beam scanning from the side of the road and obtain a three-dimensional (3-D) shape when the vehicle crosses the laser scanning section. This 3-D shape information is very useful for enhancement of the vehicle detection and axle counting. For the laser sensor in this application, there are three qualitative requirements: (i) large receiving aperture to realize high signal-to-noise ratio (SNR), (ii) wide field-of-view (FOV) to cover the detection area, and (iii) high scanning speed to realize enough spatial resolution for both scanning and vehicle moving directions. In the past, there were some scanning laser sensors used for this application, and they used coaxial optics and a polygon scanner. For this configuration, a large polygon scanner must have a large receiving aperture and obtain a high SNR. Consequently, the scanning speed must be low owing to this large scanner. For example, the scanning speed in Ref. 2 is 6 ms/line, and this means a 167-mm spatial interval for a moving speed of 100 km/h. It is obvious that this is not enough for axle counting. One of the solutions to this issue is using a scanless and wide FOV receiving optics and a small microelectromechanical system (MEMS) scanner only for transmitting the

laser beam. Using this configuration, the issue of high-speed scanning can be solved. The sensors with this concept have already been reported in Refs. 6–9. However, these sensors used the pulsed method for the TOF measurement, and the size of the photodetector must be small (generally, much less than 1 mm²) to respond to the short pulse, which is suitable for TOF measurement. Accordingly, the photodetector (and also the electrical receiving circuit) must be arrayed to realize a wide FOV and this made the sensor configuration drastically complex. This complexity is bad for everything, e.g., size, cost, performance stability, and so on. Here, we show the line scanning TOF laser sensor, which realizes all of the above-mentioned requirements, with a new simple configuration.

2 Sensor Architecture

2.1 Configuration

The sensor configuration and the photo of the optics are shown in Figs. 1 and 2, respectively. First, we describe the conceptual explanation for this sensor. The receiver is scanless and, additionally, has both a large receiving aperture and a wide FOV with only a single receiver (i.e., not arrayed). This is realized by the photodiode (PD), which has a high-aspect ratio receiving area (“high-aspect ratio PD”). This PD exists behind the receiving optics in Fig. 2, and its photo is also shown in the same figure. As with the TOF measurement method, the sinusoidal wave intensity modulation and phase difference detection are used. By using this modulation method, the problem encountered in using the high-aspect ratio PD can be prevented. The explanation for this effect is shown in detail later.

The operation of this sensor is described here. The laser beam is intensity modulated with sinusoidal wave. The

*Address all correspondence to: Masaharu Imaki, E-mail: Imaki.Masaharu@dc.MitsubishiElectric.co.jp

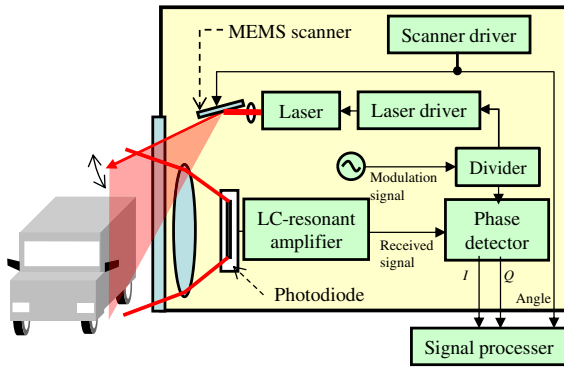


Fig. 1 Architecture of the high-speed line scanning laser sensor.

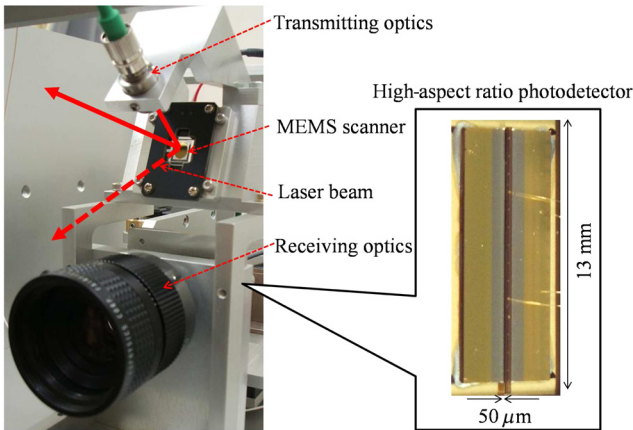


Fig. 2 Photo of the transmitter/receiver of the sensor and high-aspect ratio PD.

modulated beam is transmitted to the target (here, the vehicle and the road), and the beam is scanned using a MEMS scanner in the FOV of a scanless receiver. The backscattered light is optical-to-electrical converted by the high-aspect ratio PD through the receiving optics, and current-to-voltage converted by the trans-impedance amplifier (TIA) as the received signal. The phase difference between the modulation signal and the received one is measured by the digital phase detector. The phase detector is a type of lock-in detection. Therefore, the phase detector also acts as a notch filter for noise reduction. In the signal processor, the distance to the target (m) is measured from the phase difference and is obtained by

$$z = \frac{c}{2f_m} \times \frac{d\phi}{2\pi}, \quad (1)$$

where f_m is the modulation frequency (Hz), c is the light speed (m/s), and $d\phi$ (rad) is the phase difference between the modulation signal and the received signal. The measured data are plotted in the laser scanning area using the measured distance and the corresponding angle information. The SNR is derived from the received intensity, and the root-mean-square (RMS) error of the measured distance is predicted as

$$\Delta z \approx \frac{c}{4\pi f_m} \frac{1}{\sqrt{2\text{SNR}}}. \quad (2)$$

The description of the above equation is shown in the [Appendix](#). Note that the SNR is defined as the intensity ratio in the electrical signal domain. By using this predicted RMS error, bad measured data are screened. After this screening, the processing for the vehicle detection and axle counting is carried out. The algorithm of this processing is explained later.

The sensor parameters are shown in the following. We selected a wavelength region of $1.48 \mu\text{m}$ by considering the eye-safety. The laser diode is the one typically used as a pumping light source for an erbium-doped fiber amplifier. The laser is directly intensity modulated by a laser driver. The output average power is about 250 mW, and the modulation frequency is about 10 MHz, which corresponds to a distance ambiguity of 15 m. This ambiguity is enough for measuring a distance of up to 10 m, which is the required measurement distance in the ITS application of vehicle detection and axle counting. The output of the laser diode is coupled to a single-mode optical fiber, and the output of the fiber is collimated by transmitting optics. The diameter of the output beam is 2 mm, and the half-angle beam divergence is about 0.36 mrad. The MEMS scanner with an electromagnetic drive type is used. The laser scanning full-angle is 30 deg and the resonant frequency is 550 Hz. This corresponds to the high-speed scanning of 0.9 ms/line. This realizes a spatial resolution of 25 mm for the vehicle moving direction when the vehicle speed is 100 km/h. The sampling frequency of the phase detector (i.e., the TOF measurement interval) is about 600 kHz. This means 500 distance measurements per each line scan. It is obvious that the sensor configuration of this paper is much simpler than the arrayed receiver configuration with an element number of 550. The aperture of the receiving optics is 26.3 mm, and its focal length is 25 mm. The size of the receiving area of the device is $13 \text{ mm} \times (\text{length}) \times 50 \mu\text{m} \times (\text{width})$. The width is determined in order to make the FOV wider than the beam divergence. The length is determined to keep the sufficient frequency response at the modulation frequency of 10 MHz. The cutoff frequency of this PD itself is 30 MHz. Owing to this size, an FOV of 30 deg, which matches the laser scanning angle, is realized for the scanning direction.

The sensitivity of the high-aspect PD is 1.1 A/W. The dark current is 5 nA and is larger than the values for smaller size PDs (note that the dark current is proportional to the size). However, the dark current shot noise does not impact the noise characteristic at the output of the TIA, which is shown in [Sec. 2.2](#).

2.2 Key-Device: High-Aspect Ratio Photodiode

The high-aspect ratio PD is the key device which we have recently developed. The schematic of the cross section of this device is shown in [Fig. 3](#). We select the indium gallium arsenide (InGaAs) as the material of the device to utilize in the eye-safe wavelength region. The InGaAs absorbing layer and indium phosphorus (InP) window layer are grown on an n-type InP substrate by the metal organic chemical vapor deposition. The top surface is coated with a passivating film, which acts as an antireflection coating.

We also add a contrivance to the TIA to make use of the advantage of the high-aspect ratio PD. The PN junction capacitance, which corresponds to the capacitance between the Zn diffusion layer and the n-InP substrate layer, increases

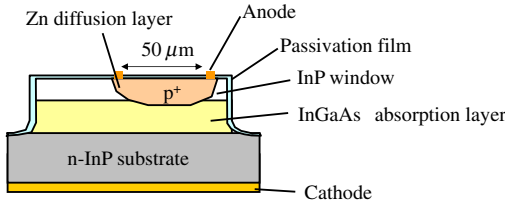


Fig. 3 Cross-sectional structure of the high-aspect ratio PD.

if the received area of the PD becomes larger. This increasing of the PN junction capacitance increases the noise level of the TIA. To prevent this problem, we applied an LC-resonant method for noise suppression. The schematic of the TIA with the LC-resonant method is shown in Fig. 4. The equivalent input noise current density i_{eq} is expressed as

$$i_{eq} = \sqrt{i_n^2 + \frac{4kT}{R_F} + \left(\frac{e_n}{R_F}\right)^2 + \left(\frac{e_n}{Z_{in}}\right)^2}, \quad (3)$$

where i_n is the input noise current density of the amplifier ($A/Hz^{1/2}$), k is the Boltzmann constant, T is the temperature of the amplifier (K), e_n is the input noise voltage density ($V/Hz^{1/2}$), R_F is the feedback resistance (ohm), and Z_{in} is the input impedance of the amplifier (ohm).

The input impedance of the amplifier Z_{in} in Eq. (3) is written as

$$Z_{in} \approx \frac{j\omega L}{1 - \omega^2 L(C_P + C_S + C_D + C_M/2)}, \quad (4)$$

where $\omega = 2\pi f$, f is the signal frequency, C_P is the PN junction capacitance of the detector (F), C_M is the common-mode capacitance of the amplifier (F), C_D is the differential input capacitance of the amplifier (F), C_S is the stray capacitance of the circuit (F), and L is the inductance (H). Without the inductor, the input impedance of the amplifier Z_{in} decreases with the increasing of the PN junction capacitance C_P , and the equivalent input noise current density i_{eq} increases. On the other hand, the input impedance becomes large at the LC-resonant frequency and the noise level can be reduced around the LC-resonant frequency. The resonant frequency is shown as follows:

$$f_r \approx \frac{1}{2\pi\sqrt{L(C_P + C_S + C_D + C_M/2)}}. \quad (5)$$

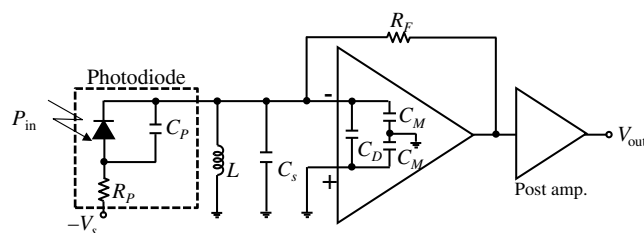


Fig. 4 Schematic of LC-resonant amplifier. V_S is bias voltage, V_{out} is the output voltage, P_{in} is the optical input power, C_p and R_p are the interterminal capacitance and resistance of the detector, respectively, C_F and R_F are the feedback capacitance and resistance, respectively, C_D and C_M are the input capacitance and common-mode capacitance of amplifier, respectively, C_S is the stray capacity of the circuit, and L is the inductance for tuning.

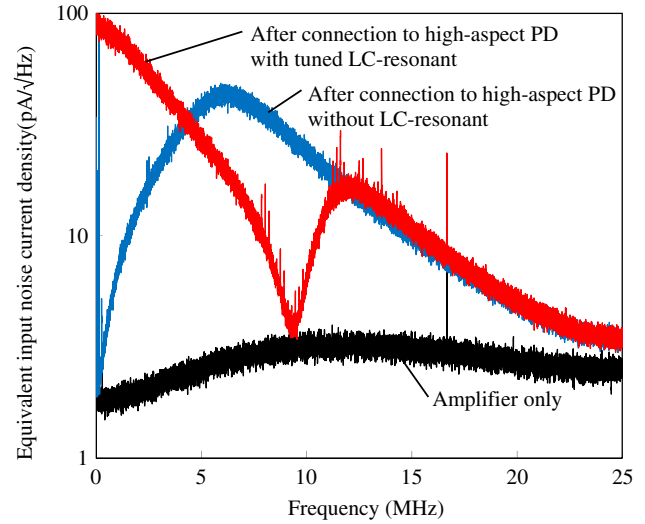


Fig. 5 Noise spectrum of an amplifier.

With the developed high-aspect ratio PD, the PN junction capacitance C_P is 72 pF. The commercial available operational amplifier is used; the common-mode capacitance is 4.5 pF, the differential input capacitance is 0.7 pF, and the stray capacitance is 10 pF. To set the resonant frequency on about 10 MHz, an inductance of 3.3 μ H was used.

Figure 5 shows the noise spectrum of the TIA, the amplifier connected with the high-aspect ratio PD without an LC-resonant circuit, and the amplifier connected with a high-aspect ratio PD with the resonant circuit. The increase in noise level of the amplifier without LC-resonant method is confirmed, but with the LC-resonant method, the reduction of the noise level is realized around 10 MHz. This noise reduction works only around the resonant frequency. This means that this noise reduction does not work if the pulsed method is used for TOF measurement since the pulsed method generally needs a wide receiving bandwidth. This is the reason why sinusoidal wave modulation is used here. By using this modulation, the receiving frequency can be unified, and the noise in the other frequency is filtered out by the phase detector. Therefore, the effect of the above-mentioned noise reduction appears distinct. The trans-impedance gain is 78 kV/A and the input noise current density of the TIA is 3.7 $pA/Hz^{1/2}$ within a 1.2-MHz bandwidth around the modulation frequency. The noise power at the output of the post amplifier is -66 dBm with a bandwidth of 1.2 MHz. In Fig. 5, it is obvious that the noise levels before and after the connection to the LC resonant to the high-aspect ratio PD are almost same around 10 MHz. This means the dark current shot noise does not impact the noise characteristic.

2.3 Key-Device: Phase Detector

The high dynamic range of the phase detector is required because there is the some target reflectance. In the case of the target reflectance is 1 and 1×10^{-3} , which corresponds to the white and black color, the order of the received electric power is 1 and 1×10^{-6} because the received optical power is changed to the current by the photodetector.

The phase detector was produced by using a field-programmable gate array because the noise characteristics with the digital phase detector are better than those of an

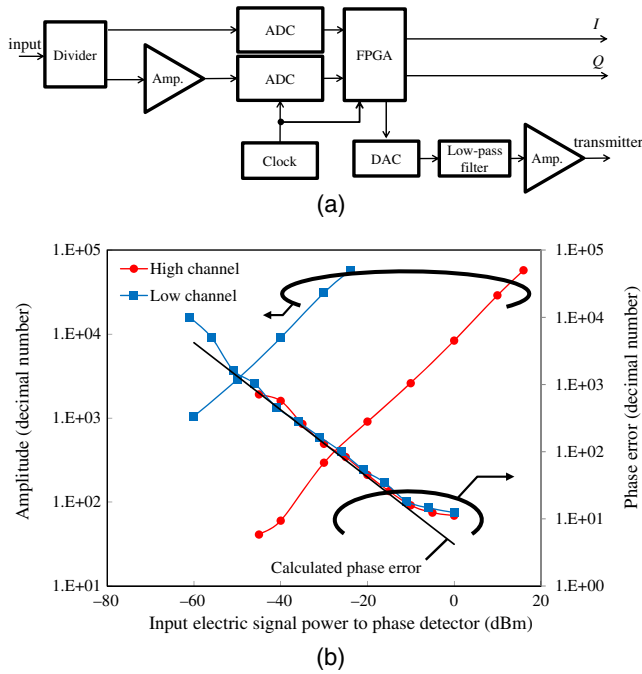


Fig. 6 The block diagram and characteristics of phase detector: (a) block diagram and (b) amplitude and phase error characteristics.

analog phase detector circuit, and a highly accurate measurement of the phase difference was realized. In addition, a high dynamic range by high- and low-input channels was developed for detecting high- and low-reflection targets such as white colored and black colored vehicles.

Figure 6(a) shows the block diagram. The input signal is divided two ways. One is the high channel at low gain and the other is the low channel at high gain. The clock in the phase detector is used for sampling of the analog-to-digital converter (ADC), and the transmitter signal whose frequency is multiplied from the clock frequency. The amplitude and RMS phase error characteristics of the phase detector are shown in Fig. 6(b). The vertical axis is a decimal number of 16 bit, and the horizontal axis is the electric input power. The range of input power is -24 to -60 dBm for the high channel, and is 16 dBm to -45 dBm for the low channel.

The calculated phase error is derived from Eq. (2) and the noise level, which is denoted in Sec. 2.2. The results are shown in Fig. 6(b). The figure shows that there is a difference of the phase error under the 100 (decimal number) between the measured and theoretical results. This difference is caused by additional error in the digital processing of the phase detector.

The RMS error of the measured distance in digital value $\Delta z'$ is written as

$$\Delta z' = \frac{c}{2 \cdot f} \frac{\Delta \phi'}{2^n}, \quad (6)$$

where c is the light speed (m/s), $\Delta \phi'$ is the phase error in a digital value (decimal number), and n is the bit number of the ADC. In this system, a 16 bit AD converter is used. For example, the amplitude is 1000 (decimal number) and the phase error is 45 (decimal number) at the high channel

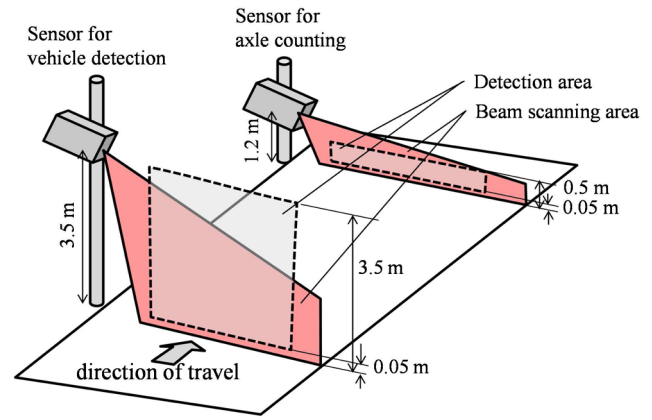


Fig. 7 Setup example of the sensor for vehicle detection and axle counting.

when the received power is -20 dBm. In this case, the RMS error of the measured distance is 1.03 cm from Eq. (6).

3 Experimental Results

The demonstration of the vehicle detection and axle counting is shown below. The sensor location is shown in Fig. 7. The sensor for vehicle detection is mounted at a 3.5-m height, and that for the axle counting is mounted at a 1.2-m height. The detection area is preset in the laser scanning area. For the vehicle detection, the corresponding height is between 0.3 and 3.5 m. For the axle counting, it is between 0.05 and 0.5 m, respectively. For each scan, the number of data for which the plot is in the detection area, is stored. If the stored number is over the threshold for 10 continuous scans, the detection flag becomes high. The threshold is 30 for the vehicle detection and 200 for the axle counting.

We tested this signal processing at the test field of Mitsubishi Electric Corporation. Figure 8 shows the demonstration of the vehicle detection: (a) the intensity image, (b) the height image, (c) the number of plots for each scan, and (d) the vehicle detection flag. The vertical and the horizontal axes are the direction of scanning for the laser beam and the number of the scanning line, respectively, and the number of horizontal pixel is 1000 in Fig. 8. In the intensity image, the white color is the high-level received signal and black color is the low-level received signal. In the height images, the target height from the ground is color-coded: blue is near the ground, red is high from the ground, and black is invalid data. The vehicle speed is about 40 km/h. The received power is -20 dBm at the body of the vehicle, and the phase error is 45 (decimal number) at the high channel in Fig. 6. The corresponding RMS error of the measured LOS distance is known from Eq. (6) as 1.03 cm. It is shown that the correct vehicle detection is performed.

Figure 9 shows the demonstration for the axle counting. The number of horizontal pixels is 1500 in Fig. 9, and the vehicle speed is about 30 km/h. The received power is -30 dBm at the tire of the vehicle, and the phase error is 131 (decimal number) at the high channel. The corresponding RMS error of the measured LOS distance is known from Eq. (6) as 3.0 cm. The vehicle is a truck that has four axles of which one is lifted. It is important to judge if the axle is lifted or not, since it reflects the load of the truck. In addition to the axles, a mudguard appeared after the second axle. Although

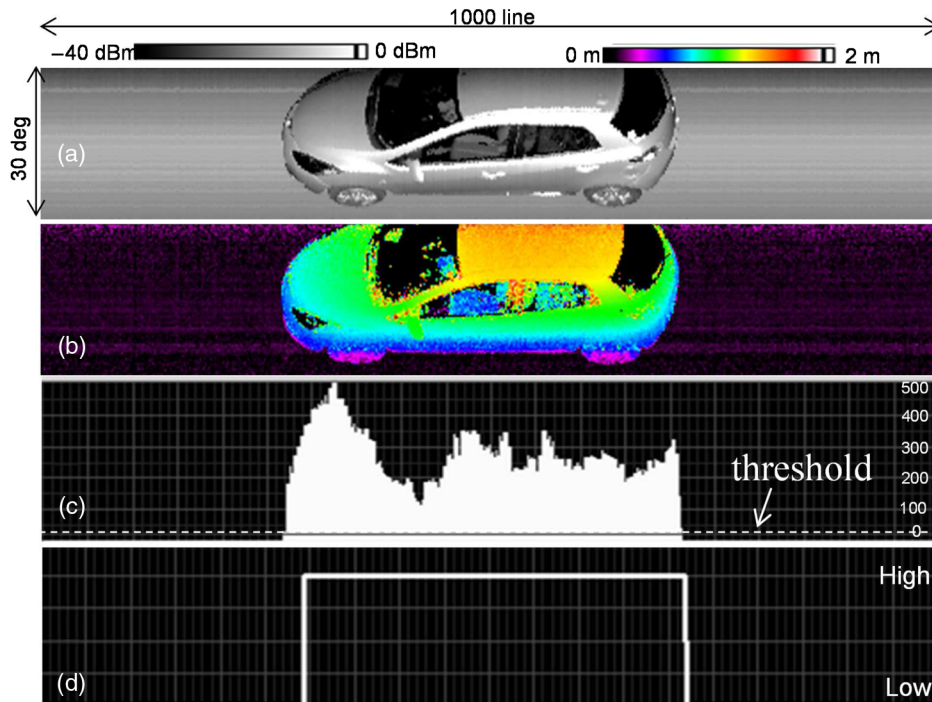


Fig. 8 Example data of the vehicle detection for silver color vehicle: (a) an intensity image, (b) a height image, (c) the valid data for vehicle detection, and (d) is the vehicle detection flag.

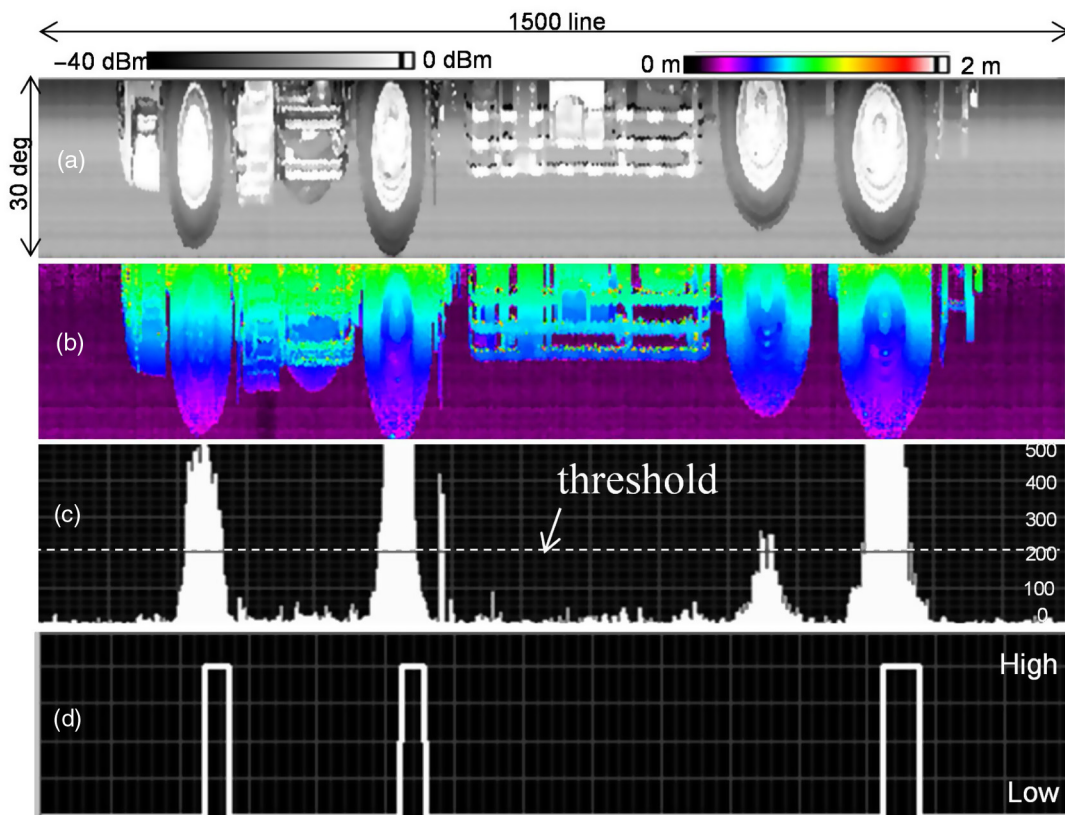


Fig. 9 Example data of the axle detection for lifted axle truck: (a) an intensity image, (b) a height image, (c) the valid data for axle detection, and (d) the axle detection flag.

a substantial amount of data corresponding to the lifted axle and mudguard are detected, these data can be omitted because the detected number does not satisfy the condition of 10 continuous scans detection. As a result, it is shown that the correct axle count is realized.

4 Summary

In conclusion, we developed the line scanning TOF laser sensor, which combines the wide FOV receiving optics and high-speed scanner with a simple configuration. The vehicle detection and axle counting, which are the important functions in ITS applications, were demonstrated. It can be seen that the sensor is optimized to realize all of (i) high SNR, (ii) high-speed scanning, (iii) wide FOV, and (iv) simple configuration, by fully combining the MEMS scanner, high-aspect ratio PD, LC-resonant TIA, and sinusoidal wave intensity modulation. The separation of signals from multiple targets is also an issue for sinusoidal wave modulation, but the influence is not so severe for the short distance measurement such as those reported in this paper. The requirement of the above-mentioned short measurable distance is true for many cases in ITS applications.

Appendix

In this section, the dependence of the RMS error of the measured distance and SNR is shown. The RMS error of the measured distance is derived from Eq. (1), and is defined as

$$\Delta z = \frac{c}{2f_m} \times \frac{\Delta\phi}{2\pi} \tag{7}$$

Figure 10 shows the schematic diagram of the signal and noise vectors when the phase of signal vector is 0. The amplitude of the signal is $\sqrt{\text{SNR}}$ when the amplitude of noise is 1. The RMS amplitude of noise in the Q -axis is $1/\sqrt{2}$. In the case of $\text{SNR} \gg 1$, the phase error is written as

$$\Delta\phi = \tan^{-1} \left(\frac{1}{\sqrt{2}} \cdot \frac{1}{\sqrt{\text{SNR}}} \right) \tag{8}$$

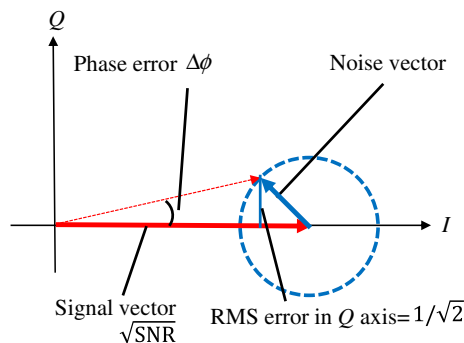


Fig. 10 Schematic diagram of signal and noise vector for I and Q phase detector.

This equation can be approximated to

$$\Delta\phi \approx \frac{1}{\sqrt{2}} \cdot \frac{1}{\sqrt{\text{SNR}}} \tag{9}$$

Equation (2) is obtained by substituting Eq. (9) to Eq. (7).

References

1. Traffic monitoring Guide, U.S. Department of Transportation (2013).
2. T. Ueda et al., "Optical axle-counting equipment," in *IEEE Conf. on Intelligent Transportation System (ITSC '97)*, pp. 326–331, IEEE (1997).
3. A. J. Chenoweth, R. E. McConnell, and R. L. Gustavson, "Overhead optical sensor for vehicle classification and axle counting," *Proc. SPIE* **3838**, 22–28 (1999).
4. H. Lee and B. Coifman, "Side-fire lidar-based vehicle classification," *Transp. Res. Rec.* **2308**, 173–183 (2012).
5. T. Sato, Y. Aoki, and Y. Takebayashi, "12249 Vehicle axle counting using two LIDARs for toll collection systems," in *ITS World Congress* (2014).
6. T. Sandner et al., "3D imaging using resonant large-aperture MEMS mirror arrays and laser distance measurement," in *IEEE/LEOS Int. Conf. on Optical MEMS and Nanophotonics* (2008).
7. B. L. Stann et al., "MEMS-scanned lidar sensor for small ground robots," *Proc. SPIE* **7684**, 76841E (2010).
8. I. Aoyagi, K. Shimokawa, and S. Kato, "2-axis MEMS scanner for a laser range finder," in *16th Int. Conf. on Optical MEMS and Nanophotonics*, p. 39 (2011).
9. C. Niclass et al., "Design and characterization of a 256 × 64-pixel single-photon imager in CMOS for a MEMS-based laser scanning time-of-flight sensor," *Opt. Express* **20**, 11863–11881 (2012).

Masaharu Imaki received his DE degree from the University of Fukui in 2005. He has been involved in the development of Doppler lidar, Raman lidar, differential absorption lidar (DIAL), and high-spectral resolution lidar in the same university. In 2007, he joined Mitsubishi Electric Corporation. His current research involves distance imaging sensor, DIAL, and Doppler lidar. He is a member of SPIE, the Japan Society of Applied Physics, the Laser Society of Japan, and the Institute of Electrical Engineers of Japan.

Shumpei Kameyama received his DE degree from Chiba University in 2011. Since 1995, he has been with Mitsubishi Electric Corporation, and he started the development of laser remote sensing systems in 1999. His current research involves coherent Doppler lidar, DIAL, and range imaging laser sensor. He is a member of the Japan Society of Applied Physics, Optical Society of America (OSA), and Institute of Electrical and Electronics Engineers (IEEE).

Eitaro Ishimura received his BS in physics from Keio University, Tokyo, Japan, in 1985. In 1985, he joined Mitsubishi Electric Corporation, Hyogo, Japan, where he has been engaged in the research and development on the high-speed photodetectors, electroabsorption modulators, and the laser diodes. Currently, he is working on optical devices for communication systems, such as low noise AlInAs avalanche photodiodes.

Masaharu Nakaji received his BS and MS degrees in electronic engineering from Nagoya Institute of Technology College, Nagoya, Japan, in 1999 and 2001, respectively. In 2001, he joined Mitsubishi Electric Corporation, Hyogo, Japan, where he has been engaged in the research and development of the high-speed photodetectors.

Hideo Yoshinaga graduated from Yokohama National University in 1992. The same year, he joined Mitsubishi Electric Corporation. He has been involved in the development of the road traffic system. He has studied the identification of the vehicle using the distance image sensor.

Yoshihito Hirano received his DE degree from Osaka University in 2001. Since 1985, he has been with Mitsubishi Electric Corporation and started the research on optical communication equipment, solid-state lasers, nonlinear optics, laser radars, and microwave photonics. He is a member of the Japan Society of Applied Physics, the Laser Society of Japan, the IEEE of Japan, and the OSA. He is also a senior member of IEEE/Lasers and Electro-Optics Society.